IEEE Access
Multidisciplinary ⋮ Rapid Review ⋮ Open Access Journal

Received 12 September 2022, accepted 21 September 2022, date of publication 3 October 2022, date of current version 11 October 2022.

Digital Object Identifier 10.1109/ACCESS.2022.3211525

RESEARCH ARTICLE

Hand Blockage Impact on 5G mmWave Beam Management Performance

FILIPA FERNANDES[1], (Member, IEEE), CHRISTIAN ROM[2], JOHANNES HARREBEK[2], SIMON SVENDSEN[2], AND CARLES NAVARRO MANCHÓN[1]

[1]Department of Electronic Systems, Aalborg University, 9220 Aalborg, Denmark
[2]Nokia, 9220 Aalborg, Denmark

Corresponding author: Filipa Fernandes (fsdsf@es.aau.dk)

ABSTRACT Modelling and managing user-induced rotation and blockage in handheld multi-antenna panel devices are some of the pivotal challenges of future narrow beam millimeter wave (mmWave) communications. While studies have been conducted separately on multi-panel beam management (BM) performance and mmWave user blockage loss, no study has been made to date, to the best of the authors' knowledge, on how hand blockage influences beam alignment accuracy in the context of 5G new radio (NR). This paper presents a link-level evaluation on the impact of user hand grip in BM performance under a 5G NR standard compliant signalling and measurement framework. A high-detail handset model is employed, equipped with multiple panels and different hand grips obtained with CST Microwave Studio, a 3D electromagnetic field simulation tool. Additionally, this study incorporates aspects such as intra-cell mobility, device rotation, hand grip variability and changing propagation conditions. Results show that hand blockage can significantly degrade beam alignment performance, particularly for dual-hand grips in predominantly line-of-sight (LOS) environments. Finally, results suggest that the current blockage model proposed by 3GPP must be further enhanced to account for blockage on a per-panel basis. This would allow a more accurate portrayal of user hand behaviour, which would support the analysis and design of effective solutions to overcome the user's unpredictable shadowing effects at mmWave frequencies.

INDEX TERMS 5G NR, beam management, hand blockage, mmWave, multi-panel.

I. INTRODUCTION

While 5th Generation of mobile networks (5G) relies on millimeter wave (mmWave)'s large spectrum availability to enable data-hungry applications, its poor propagation conditions require that narrow beams be employed, both on the next generation node base station (gNodeB) and user equipment (UE), to improve overall link budget. However, the directional nature of these antennas, along with unpredictable device orientation, create the need for multi-panel integration on the UE side [1]. This adds a higher degree of complexity to the beam alignment procedure, being considered as one of the big challenges for beam management (BM) in future 5G and 6th Generation of mobile networks (6G) releases [2], [3]. Additionally, at these high frequencies, the impact of the user on device performance also extends to self-blockage effects. Besides blockage from surrounding buildings, people or vehicles heightened by the use of narrower beams, the user's body itself will increase impedance mismatch, energy absorption and most significantly, shadowing effects. Therefore, the user's proximity to the device will manifest negatively in the UE's radiation performance, becoming an additional hindrance to the feasibility of mmWave communication systems.

Though both these fronts have been separately investigated, a study is still missing on exploring the BM procedure performance in conjunction with mmWave user blockage. This paper intends to fill this gap in the literature by assessing the impact of human hand gripping on the performance of link-level mmWave BM. A detailed simulation tool has been created with a multitude of features that aim to recreate realistic scenarios for mmWave communications. These features,

The associate editor coordinating the review of this manuscript and approving it for publication was Vlad Diaconita.

which can also be listed as the main contributions of this work, include:

- BM performance evaluation for initial beam alignment based on the 3rd generation partnership project (3GPP)-defined downlink (DL) signalling and measurement framework in which future 5G deployments for mmWave will be based on.
- Introduction of intra-cell user mobility, device rotation and variable channel conditions to achieve challenging outdoor simulation environments.
- Design of a multi-panel UE with beamforming capabilities. Most works on multi-panel UEs assume a single wide beam per panel (see Section I-A). However, future mmWave device implementations will use narrow beams, further complicating the beam alignment process. Therefore, it is important to consider this aspect when evaluating BM performance.
- Usage of a 3D electromagnetic simulation tool to produce a detailed model of the antenna arrays, UE form factor (with a metal chassis, plastic case and glass layers) and the grips used to represent user hand blockage. In this work Computer Simulation Technology (CST) Microwave Studio [4] is employed to capture the effects of the form factor and the user's hand on the radiation performance of mmWave antennas that cause the loss of shape of the original codebook beams. While usually overlooked in the literature, results show that this phenomenon can actually significantly degrade the BM procedure, particularly in line-of-sight (LOS) environments.
- Adoption of three commonly used hand grips portraying different hand positions and grip tightness levels that could correspond, for example, to a user performing a video call, streaming or gaming on their smartphone. This results in a range of distinct blockage levels over each panel, to ensure that hand blockage is fairly depicted in both optimistic and pessimistic scenarios.
- Incorporation of the 3GPP blockage model in the tool for comparison with the CST model employed regarding their impact on beam alignment accuracy. Through this work it is evident that the 3GPP model leads to an overly pessimistic performance degradation when compared to the CST model, mostly due to its flat attenuation region approach. Results suggest that the introduction of panel-based blockage to the current 3GPP model could be a step towards improving its hand grip blockage characterization.

In summary, this work focuses on integrating a highly detailed model of the antennas, the smartphone and the user's hand itself in a link-level BM performance analysis. It is important to note that this CST-based model introduces an additional level of complexity that, allied with all the other features mentioned above, provide a level of realism to the system that precludes a theoretical analysis of its performance, hence why Monte Carlo simulations are employed instead. This study is meant to complement other works in the literature such as [5] and [6], that employ extensive analytical performance analysis with simplified assumptions on propagation, signalling or handset models.

A. RELATED WORKS

Extensive work on BM performance assessment has been done incorporating multi-panel UEs. The authors in [7] highlight the performance improvement of mmWave UE multi-panel uplink transmission when compared to its omni-directional counterpart under 5G-compliant system level simulations. A mmWave system level performance evaluation is conducted in [8] employing 5G new radio (NR) BM procedures and a proposed UE panel switching mechanism that maintains beam alignment errors low even for higher speeds. In [9] the authors explore the potential vulnerabilities of the multi-panel design for mobility purposes in a scenario where updated beam information might not reach all panels simultaneously. It is worth noting that these studies assume single antenna element panels, without beamforming on the UE side. In [10] a particle filter is used to improve beam alignment performance by combining reference signal received power (RSRP) measurements for a multi-panel array equipped device with orientation information obtained from inertial measurement unit sensors. A machine learning approach for the same method is proposed in [11] to further boost beam-prediction accuracy. However, the listed works on mmWave BM performance do not factor in user blockage into their studies.

Several works have also been developed to quantify and model human blockage. Some of these approaches include mathematical models where the blockage loss is calculated through the diffracted fields across the body, modeled as a conducting cylinder [12] or a combination of absorbing screens mimicking different body parts [13]. Other papers resort to heuristic models based on electromagnetic simulations and real-life phantom and device measurements that evaluate this blockage in terms of realized gain or equivalent isotropic radiated power-based spherical coverage, as well as received signal strength (RSS) through ray-tracing tools for outdoor urban environments [14], [15], [16], [17], [18]. Most of these works register full body blockage losses ranging from 20 dB to 35 dB, focusing mostly on the effects of the user's torso with only 2 simplified hand grips: portrait and landscape, depending on the phone's orientations. The large discrepancy in the loss values can be explained by the lack of consistency within research on antenna types and design, form factor implementation, user stance or gripping assumptions, since there is still no common agreement on how to model all of these complex components. In an attempt to reach a consensus and achieve result replicability, 3GPP proposes a model in [19] that attributes a flat attenuation of 30 dB to a region of the angular space delimited by the phone's orientation. This simplistic modelling has been challenged in works like [20] that propose instead a statistical model to approximate the attenuation of the same self-user blockage

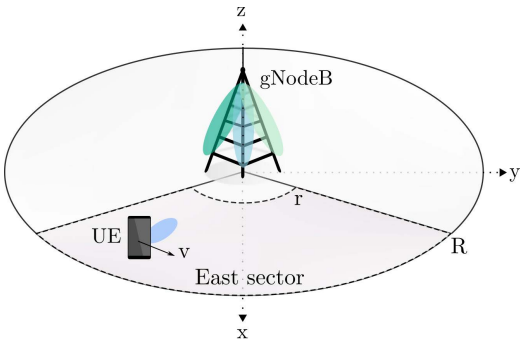

FIGURE 1. Network layout.

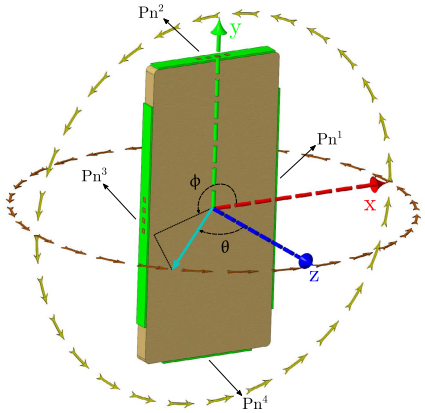

FIGURE 2. UE's local coordinate system (LCS), panel placement and spherical coordinates. Pn^i indicates the position of the ith antenna panel.

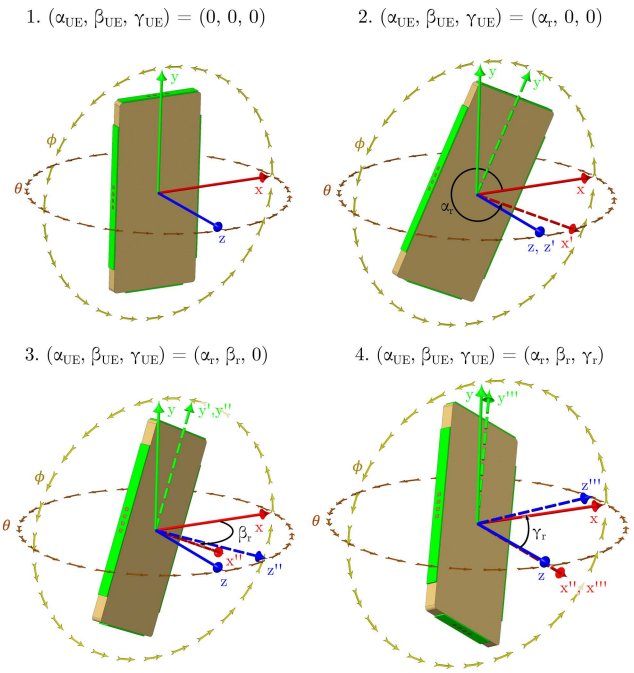

FIGURE 3. LCS (dotted axes) orientation with respect to the GCS (solid axes) through a sequence of 3 rotations: $\alpha_r = \frac{11\pi}{6}$, $\beta_r = -\frac{\pi}{6}$ and $\gamma_r = \frac{\pi}{6}$.

loss region to a Gaussian distribution, making the distinction between body and hand grip blockage. In [21] an exhaustive study is conducted to characterize hand and body blockage on a commercial mmWave device that shows blockage is dependent on factors such as antenna type, tightness of hand grip and narrow beams. Based on this, smaller regions of interest are defined in the angular space, based on where significant blockage is experienced, leading the authors to conclude that blockage loss can be considerably lower than claimed in previous papers, registering loss values for hand gripping as low as 5 dB.

B. ORGANIZATION

The remainder of this paper is organized as follows: Section II describes the system model, while Section III and IV focus on describing and comparing the two approaches used to model self-blockage in this study. Section V illustrates the results of blockage impact on BM performance and Section VI concludes the paper and reflects on possible solutions to incorporate more detailed representation of self-blockage in current models.

II. SYSTEM MODEL

Fig. 1 displays the DL single-cell mmWave system considered in this work, where intra-cell BM operations take place to achieve initial beam alignment between the gNodeB and a moving user. A tri-sector cell is assumed, where the user moves linearly with a fixed orientation and speed v in the east sector, bounded by mobility ranges r and R. The gNodeB, standing at a height of h_t m, is equipped with a uniform planar array (UPA) of N_t patch antennas. The UE, being held at a height of h_r m, is modeled as a multi-panel device, each panel composed of a uniform linear array (ULA) of N_r patch antennas. Due to the limited angular coverage of these antennas, its panel placement follows a commonly used edge design [22], with one antenna module on each side of the form factor, as can be seen in Fig. 2.

The gNodeB and UE positioning can be described according to the global coordinate system (GCS) represented in Fig. 1, while their orientation is dictated by their own LCS, expressing any 3D rotation with respect to the GCS. Although the gNodeB is assumed to have a fixed location, with its LCS aligned with the GCS, the UE's orientation varies over the bearing angle α_{UE}, the downtilt angle β_{UE} and the slant angle γ_{UE}. As illustrated in Fig. 3, this set of angles represents three elemental rotations about the z, y and x axes, respectively [19]. In this work two distinct device orientation modes are considered for the UE: portrait and landscape. Portrait mode takes $\beta_{UE} = 0$ with α_{UE} and γ_{UE} varying randomly according to a uniform distribution in the ranges $\alpha_{UE} \in [0, 2\pi]$ and $\gamma_{UE} \in [0, \frac{\pi}{2}]$. In turn, landscape mode takes $\gamma_{UE} = 0$ with α_{UE} and β_{UE} varying randomly according to a uniform distribution in the ranges $\alpha_{UE} \in [0, 2\pi]$ and $\beta_{UE} \in [-\frac{\pi}{2}, 0]$.

A. CHANNEL MODEL

The mmWave DL channel response is obtained for the ith UE panel through QUAsi Deterministic RadIo channel GenerAtor (QuaDRiGa), a 3GPP compliant, 3D geometry-based stochastic channel model generator [23], modelled in the kth time-frequency resource as

$$\boldsymbol{H}^i(k) = \sum_{l=1}^{L} g_l \boldsymbol{a}_r^i(\theta_{r,l}^i, \phi_{r,l}^i)\boldsymbol{a}_t^H(\theta_{t,l}, \phi_{t,l})e^{-j2\pi\tau_l f_k} \quad (1)$$

with L, g_l, τ_l and f_k being the total multipath components of the channel, the path l's complex gain and delay values and the subcarrier frequency, respectively. Additionally, $\boldsymbol{a}_t$ and $\boldsymbol{a}_r^i$ express the transmitter and receiver array responses for a path l's elevation and azimuth angles of arrival $(\theta_{r,l}^i, \phi_{r,l}^i)$, and departure, $(\theta_{t,l}, \phi_{t,l})$.[1] The array response for a gNodeB or UE array panel of size $N = N_x N_y N_z$ is written as

$$\boldsymbol{a}(\theta, \phi) = \tilde{\boldsymbol{a}}(\theta, \phi) \odot \boldsymbol{g_{ae}}(\theta, \phi) \quad (2)$$

where $\boldsymbol{g_{ae}} \in \mathbb{C}^N$ denotes each antenna element's linear gain, $\odot$ the Hadamard product and $\tilde{\boldsymbol{a}}$ is described as

$$\tilde{\boldsymbol{a}}(\theta, \phi) = \frac{1}{\sqrt{N}}\boldsymbol{a}_z(\theta) \otimes \boldsymbol{a}_y(\theta, \phi) \otimes \boldsymbol{a}_x(\theta, \phi) \quad (3)$$

where $\otimes$ expresses the Kronecker product, with $\boldsymbol{a_x} \in \mathbb{C}^{N_x}$, $\boldsymbol{a_y} \in \mathbb{C}^{N_y}$ and $\boldsymbol{a_z} \in \mathbb{C}^{N_z}$ given by

$$\boldsymbol{a_x}(\theta, \phi) = [1, e^{j\pi \sin\theta\cos\phi}, \ldots, e^{j\pi(N_x-1)\sin\theta\cos\phi}]^T \quad (4)$$

$$\boldsymbol{a_y}(\theta, \phi) = [1, e^{j\pi \sin\theta\sin\phi}, \ldots, e^{j\pi(N_y-1)\sin\theta\sin\phi}]^T \quad (5)$$

$$\boldsymbol{a_z}(\theta) = [1, e^{j\pi \cos\theta}, \ldots, e^{j\pi(N_z-1)\cos\theta}]^T. \quad (6)$$

B. SIGNAL MODEL

The signal model employed in this paper is based on the current DL signalling proposed by 3GPP for BM, which is described below.

1) BM PROCEDURES - P1, P2 AND P3

3GPP's BM framework is described as a set of layer 1 (L1) and layer 2 (L2) procedures that employ beam sweeping, beam measurement, beam determination and beam reporting to achieve and maintain beam alignment between the gNodeB's and the UE's narrow beams [24], [25]. The procedures in question are not specified in the standard but are colloquially referred to as P1, P2 and P3 in technical discussions and reports [24]. P1 refers to the gNodeB beam selection in an initial access (IA) context where broad beams are typically used to scan the angular space and estimate a coarse serving direction for a user. P2 takes place after P1, where the gNodeB uses narrower beams to refine the former beam selection within the broad beam direction. Finally, P3 occurs after beam selection at the gNodeB side where, with a fixed transmitting beam, the UE can sweep through its beams to find the best beam pair.

[1] The reader should note that L, g_l, τ_l, departure and arrival angles are considered to be time-varying. However, to simplify notation, the dependency of these channel parameters with the time-frequency index k is omitted in (1).

It is worth noting that the standard does not mandate that all of these conceptual procedures be instated. Similarly, the beamwidth relationship described above between P1 and P2 beams, despite being a common assumption in the industry, is not specified in the standard. Instead, this should be scenario-dependent to avoid unnecessary latency and signalling overhead. Therefore, this work employs a variation of these procedures, achieving beam alignment through P1 with narrow beams on the gNodeB side and P3 at the UE, eliminating the need for P2 beam refinement. Two stages are defined for this process: first, a joint gNodeB beam and UE panel selection, followed by a UE panel beam refinement, as detailed in Fig. 4.

For both P1 and P3, the received signal at any UE panel i in the kth time-frequency resource is given by

$$y^i(k) = \boldsymbol{w}^{iH}\boldsymbol{H}^i(k)\boldsymbol{f}x(k) + \boldsymbol{w}^{iH}\boldsymbol{n}^i(k) \quad (7)$$

where $\boldsymbol{H}^i(k) \in \mathbb{C}^{N_r \times N_t}$ denotes the channel matrix for UE panel i as defined in (1). $\boldsymbol{f} \in \mathbb{C}^{N_t}$ is the gNodeB beamforming vector containing the analog phase shifts for a beam, with a constant modulus of $\frac{1}{\sqrt{N_t}}$, that spatially filters the transmitted signal $x(k)$. This signal is received at the UE with a beam defined by the analog phase shifts in the beamforming vector $\boldsymbol{w}^i \in \mathbb{C}^{N_r}$, with a constant modulus of $\frac{1}{\sqrt{N_r}}$. Finally, $\boldsymbol{n}^i(k) \in \mathbb{C}^{N_r} \backsim \mathcal{CN}(\boldsymbol{0}, \sigma^2\boldsymbol{I})$ is the receiver's noise in the kth time-frequency resource modeled as a complex additive white Gaussian noise (AWGN) vector with variance σ^2. This work assumes perfect subcarrier orthogonality conditions, where the maximum channel delay response is within the cyclic prefix duration and the channel response remains constant during a full orthogonal frequency-division multiplexing (OFDM) symbol.

2) P1 - JOINT gNodeB BEAM AND UE PANEL SELECTION

In this stage, the gNodeB sweeps through N_{ss} narrow beams selected from the gNodeB codebook $\mathcal{C}_t$ (see Section II-C1), each associated with a distinct synchronization signal block (SSB). SSBs are sets of resources spanning 4 OFDM symbols in time and 240 subcarriers in frequency, generally used for L1-RSRP measurements to determine the best gNodeB serving beam. One or multiple SSBs compose an SSBurst, which is transmitted according to a numerology-dependent transmission pattern [26], [27]. The SSBurst generation is performed through MATLAB®'s 5G Toolbox™ [28]. In P1, the UE activates a single antenna element per panel, receiving and measuring these signals with a wide beam. For this purpose, a broad beam combining vector is employed $\boldsymbol{w}_{\psi_{r,b}} \in \mathbb{C}^{N_r}$, where all entries are null except for the first one, which takes a unit value. It is assumed that the UE activates all its panels simultaneously for measurement purposes, following 3GPP's "Assumption-2" (MPUE A2) or "Assumption-3" (MPUE A3) [29]. For each received SSB associated to a beam ψ_t, the UE measures its secondary synchronization (SS)-RSRP at each of the panels [30]. This is the linear average over the power contributions (in W) of the resource

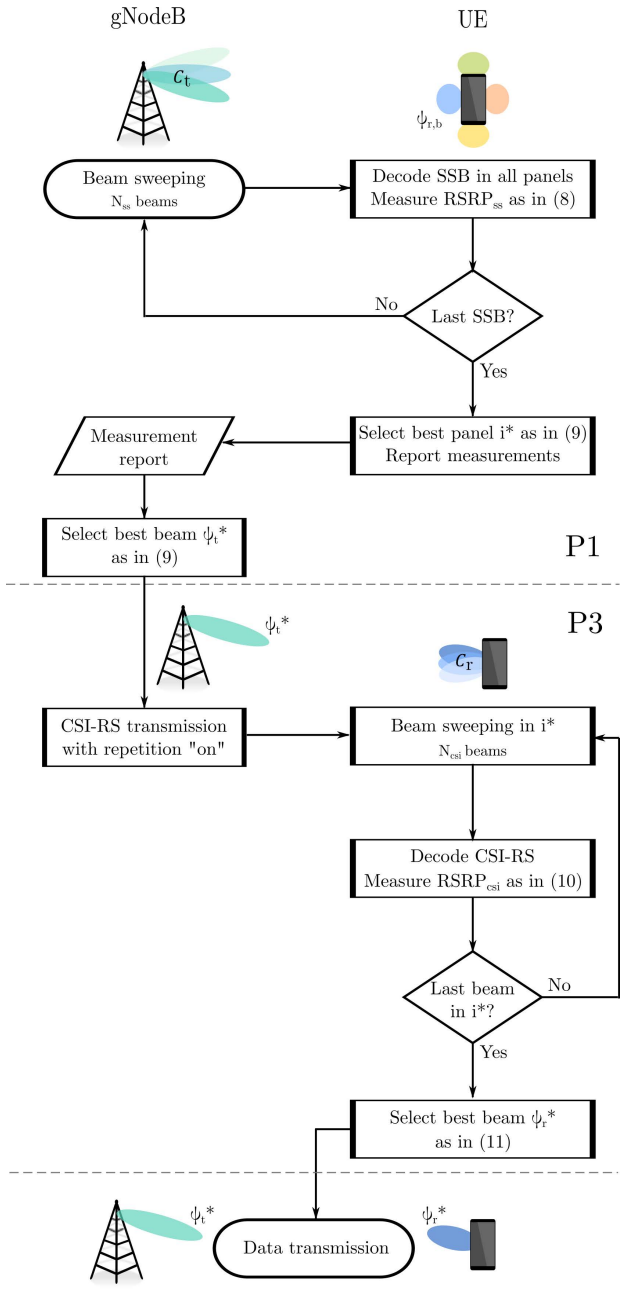

FIGURE 4. Flowchart of adopted 3GPP-based BM process.

data set $\mathcal{K}_{ss}$ within that SSB that carries the SS signals. Thus, for panel i and beam ψ_t, the RSRP measurement is computed as

$$RSRP_{ss}(\psi_t, i) = \frac{1}{|\mathcal{K}_{ss}|} \sum_{k \in \mathcal{K}_{ss}} |\boldsymbol{w}_{\psi_{r,b}}^H \boldsymbol{H}^i(k) \boldsymbol{f}_{\psi_t} + \boldsymbol{w}_{\psi_{r,b}}^H \boldsymbol{n}^i(k)|^2 \tag{8}$$

where $|\mathcal{K}_{ss}|$ refers to the total amount of time-frequency resources from the SSB transmitted by beam ψ_t containing SS signals. After obtaining $RSRP_{ss}$ for all the beams, it is assumed that the UE decides on the best selected panel $i^\star$ to keep active for data transmission and reports a subset of the highest power transmit beams back to the gNodeB for selection of the best beam $\psi_t^\star$. This joint gNodeB beam and UE panel selection results thus in

$$(\psi_t^\star, i^\star) = \arg\max_{\psi_t, i}(RSRP_{ss}(\psi_t, i)). \tag{9}$$

3) P3 - UE BEAM PANEL SELECTION

Once $\psi_t^\star$ has been determined on the gNodeB side, it is then used to send N_{csi} Channel State Information Reference Signal (CSI-RS) to the UE, one for each UE beam, to initiate beam refinement on the receiver side. CSI-RS are UE-specific signals transmitted by the gNodeB to monitor radio link channel characteristics for several use cases. These signals have an extremely flexible configuration, tailored to each diverse application. This work focuses on their role for DL BM, to obtain L1-RSRP measurements for UE beam candidate selection [25]. In this particular case, CSI-RS are distinguished with an additional higher layer parameter named "repetition" which has a binary "on" or "off" state. In P3 this parameter is set to "on", meaning that the UE can assume that no sweeping is being done on the gNodeB side and, therefore, can sweep through its own beams in panel $i^\star$, which are selected from the UE codebook $\mathcal{C}_r$ (see Section II-C2). When received at the UE, with a beam ψ_r, its channel state information (CSI)-RSRP is measured, in an analogous process to the one described in (8), over the resource elements that carry CSI-RS so that

$$RSRP_{csi}(\psi_r) = \frac{1}{|\mathcal{K}_{csi}|} \sum_{k \in \mathcal{K}_{csi}} |\boldsymbol{w}_{\psi_r}^H \boldsymbol{H}^{i^\star}(k) \boldsymbol{f}_{\psi_t^\star} + \boldsymbol{w}_{\psi_r}^H \boldsymbol{n}(k)|^2. \tag{10}$$

This is repeated for all the beams in the panel to allow the UE to complete the beam alignment procedure by selecting the beam with the highest power level, indicated by

$$\psi_r^\star = \arg\max_{\psi_r}(RSRP_{csi}(\psi_r)). \tag{11}$$

C. BEAMFORMING CODEBOOK

1) gNodeB CODEBOOK

To ensure sufficient signal strength for any user position, the cell sector's coverage range is divided into two smaller regions, coverage range 1 (CR1) and coverage range 2 (CR2), as seen in Fig. 5. A user located in CR1 is closer to the gNodeB while a user in CR2 is nearer to cell-edge. The UE's initial position and trajectory direction follow a uniform distribution in the xy plane (since the user's height in the z-axis is kept constant) within the cell sector's area. For the purpose of this study, it is worth highlighting that the UE's mobility is restricted to the bounds of the cell sector r and R, always remaining within the coverage range.

For beam sweeping at the gNodeB, a directional beamforming codebook is adopted, dividing the cell's sector coverage into angular regions in azimuth and elevation. These beams belong to a predefined, finite set of N_{ss} vectors $\mathcal{C}_t = \{\boldsymbol{f}_{\psi_t} | \psi_t = 1, \ldots, N_{ss}\}$ which is referred to henceforth as the

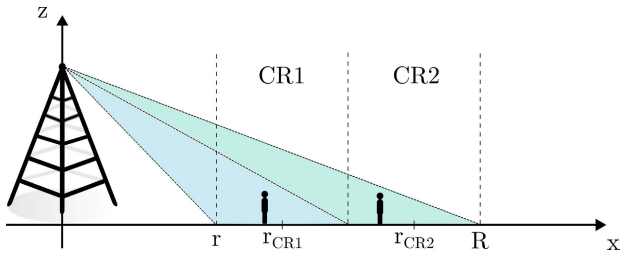

FIGURE 5. Cell coverage regions for gNodeB grid of beams (GoB) design.

gNodeB codebook. The array steering vector for a transmit beam ψ_t pointing towards $(\theta_{\psi_t}, \phi_{\psi_t})$ is defined in the ψ_t^{th} vector of the codebook as

$$\boldsymbol{f}_{\psi_t} = \boldsymbol{a}_t(\theta_{\psi_t}, \phi_{\psi_t}). \tag{12}$$

In CR1, due to the UE's proximity to the gNodeB, N_{ss}^{CR1} wider beams are employed while users in CR2 require N_{ss}^{CR2} more directive beams to compensate for pathloss. Since these higher gain beams are also narrower, to cover the same angular coverage area, it is assumed that $N_{ss}^{CR1} < N_{ss}^{CR2}$. Therefore, this codebook describes a grid of beams (GoB) composed of $N_{ss} = N_{ss}^{CR1} + N_{ss}^{CR2}$ beams. For a given range CR, the azimuth steering angles, $\phi_{\psi_t}^{CR}$, are linearly spaced within the angular range of the sector such that

$$\phi_{\psi_t}^{CR} = -\frac{\pi}{3} + (\psi_t^{CR} - 1) \times \frac{2\pi}{3x(N_{ss}^{CR} - 1)}, \ \psi_t^{CR} = 1, \ldots, N_{ss}^{CR}. \tag{13}$$

Moreover, all the beams of a common CR share an elevation steering angle, $\theta_{\psi_t}^{CR}$, defined as

$$\theta_{\psi_t}^{CR} = \pi - \arctan\left(\frac{r_{CR}}{h_t - h_r}\right) \tag{14}$$

where r_{CR} represents the center of the coverage region's radius. Both regions are assumed to have the same coverage range. The radius of $CR1$ is given by

$$r_{CR1} = r + \frac{R - r}{4} \tag{15}$$

and the radius of $CR2$ is described as

$$r_{CR2} = r + \frac{3(R - r)}{4}. \tag{16}$$

2) UE PANEL CODEBOOK

Each panel integrated into the device is considered to have beamforming capabilities for UE beam refinement. Each panel produces a finite set of N_{csi} vectors $\mathcal{C}_r = \{\boldsymbol{w}_{\psi_r} | \psi_r = 1, \ldots, N_{csi}\}$, the UE panel codebook. The array steering vector in any panel for a receive beam ψ_r directed towards $(\frac{\pi}{2}, \phi_{\psi_r})$ is expressed as

$$\boldsymbol{w}_{\psi_r} = \boldsymbol{a}_r(\frac{\pi}{2}, \phi_{\psi_r}). \tag{17}$$

Each ULA panel in the UE covers a $\frac{\pi}{2}$ sector of the angular space in the azimuth domain, with linearly spaced steering angles ϕ_r such that

$$\phi_{\psi_r} = -\frac{\pi}{4} + (\psi_r - 1) \times \frac{\pi}{2 \times (N_{csi} - 1)}, \quad \psi_r = 1, \ldots, N_{csi}. \tag{18}$$

TABLE 1. 3GPP gNodeB and UE antenna modelling.

Parameter	gNodeB	UE
$\theta_{3\,\mathrm{dB}}$	65°	90°
$\phi_{3\,\mathrm{dB}}$		
SLA_v	30 dB	25 dB
A_m		
$\max\{G_{ae}\}$	8 dBi	5 dBi

III. ANTENNA AND HAND BLOCKAGE MODEL

This work focuses on assessing how BM performance is impacted by user hand-grip induced blockage in a multi-panel handset terminal. To achieve this, two models are adopted for human blockage: a simplified model proposed by 3GPP and a highly detailed model of the smartphone antenna integration and hand gripping obtained through CST Microwave Studio [4]. The contrast between these two models comes down to the values that the entries of the vector $\boldsymbol{g_{ae}}$ take in (2), defined in Section II-A. Both models, linked to a common codebook choice, are compared in Section IV, whereas their influence in BM performance is analyzed in Section V.

A. 3GPP MODEL

1) gNodeB AND UE ANTENNA MODELLING

3GPP defines in [31] a generalized antenna radiation pattern model resembling a patch antenna. It's vertical radiation pattern, in dB, is given by

$$G_{ae,v}(\theta) = -\min\{12\left(\frac{\theta - 90°}{\theta_{3\,\mathrm{dB}}}\right)^2, SLA_v\}, \tag{19}$$

where $\theta_{3\,\mathrm{dB}}$ and SLA_v are the vertical half power beamwidth and the side lobe suppression value. Similarly, the horizontal antenna element radiation pattern is expressed in dB as

$$G_{ae,h}(\phi) = -\min\{12\left(\frac{\phi}{\phi_{3\,\mathrm{dB}}}\right)^2, A_m\}, \tag{20}$$

with $\phi_{3\,\mathrm{dB}}$ and A_m being the horizontal half power beamwidth and the front to back ratio of the radiation pattern. Finally, the 3D antenna element radiation pattern is computed as

$$G_{ae}(\theta, \phi) = -\min\{-[G_{ae,v}(\theta) + G_{ae,h}(\phi)], A_m\}. \tag{21}$$

The same model is considered both at the gNodeB and UE with their own parametrization defined in Table 1. The antenna arrays are constructed with this model assuming a half-wavelength spacing between antenna elements. For the UE, 4 identical ULA arrays are employed and rotated $90° \times (i - 1)$ degrees, to mimic the relative orientation of a panel Pn^i in the LCS.

TABLE 2. 3GPP self-blocking region parameters.

Mode	ϕ_{sb}	x_{sb}	θ_{sb}	y_{sb}
Portrait	260^o	120^o	100^o	80^o
Landscape	40^o	160^o	110^o	75^o

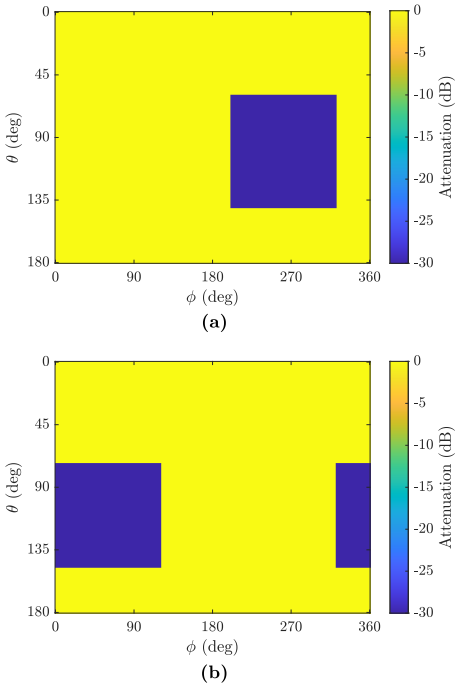

FIGURE 6. Stereographic projection of 3GPP's self-blocking attenuation region. (a) Portrait mode. (b) Landscape mode.

2) SELF-BLOCKING MODEL

Two distinct blockage models are detailed in [19], model A and model B. Model A in particular assumes a stochastic approach to characterize human and vehicular blocking, including a self-blocking component. This feature mimics the user's blockage by creating an attenuation region in the UE's LCS for a device oriented in portrait or landscape mode. These self-blocking regions, described in Table 2, depict a central blockage direction, (θ_{sb}, ϕ_{sb}), that spans x_{sb} and y_{sb} degrees in azimuth and elevation, respectively. This 3GPP-defined self-blocking model proposes a binary attenuation, where every direction within the self-blocking region suffers a 30 dB loss, while the rest of the angular space remains with 0 dB attenuation, as depicted in Fig. 6 for each of the UE orientation modes.

B. CST MODEL

1) FORM FACTOR MODELING

The form factor simulated resembles a commonly adopted wide-body design with a width, length and thickness of 76 mm, 157 mm and 10 mm, respectively. At mmWave frequencies, the performance of smartphone-integrated antennas is much more susceptible to deterioration due to proximity to other elements contained in the form factor, such as

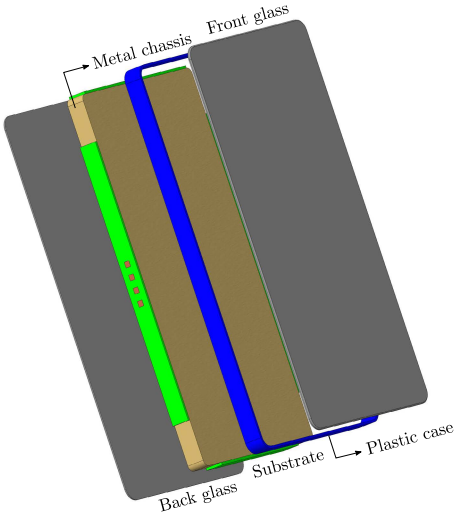

FIGURE 7. CST-modeled form factor.

TABLE 3. Dielectric constant (ε_r), loss tangent ($\tan\delta$) and electrical conductivity (σ) of the CST model components at 28 GHz.

Component	Material	ε_r	$\tan\delta$	σ (S m^{-1})
Chassis	Copper	-	-	5.8
Substrate	Rogers 4003	3.55	0.0027	-
Case	Plastic	2.9	0.0075	-
Glass	-	5.75	0.0036	-
User hand	-	16.5	-	25.8

cameras, glass displays or microphones. In order to exclude the impact of design-specific placement of these components to produce a more generic result set, a simplified form factor is considered in Fig. 7. It is composed of a solid metal chassis surrounded by a 1 mm thick substrate layer and plastic frame, with the front and the back glass components of the device included. These materials' properties, at the operation frequency of 28 GHz, are summarized in Table 3.

2) UE ANTENNA MODELING

A patch antenna is designed with CST to imitate the 3GPP UE model described in Section III-A1. Each element is simulated as a dual-polarized patch antenna occupying an area of 2.4 mm × 2.4 mm, using the device's chassis as a ground plane and a substrate 1 mm thick. For this study, only one of the polarizations is employed. Assuming a half-wavelength spacing between antenna elements, these patches are simulated as part of 4 distinct ULA arrays integrated at the center of each edge of the form factor, as can be seen in Fig. 2.

3) HAND GRIP MODELING

This work considers three representative hand grips for self-blocking, one for the phone in portrait mode and two for the phone in landscape mode. Fig. 8 represents a right hand grip over the phone in portrait mode. The user's thumb is placed over Pn^1 and three fingers clasp the device in close proximity to Pn^3. This position is commonly used during

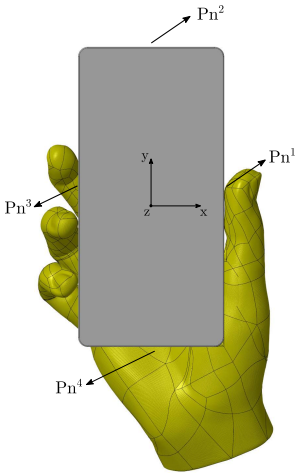

FIGURE 8. Right hand grip model - portrait mode.

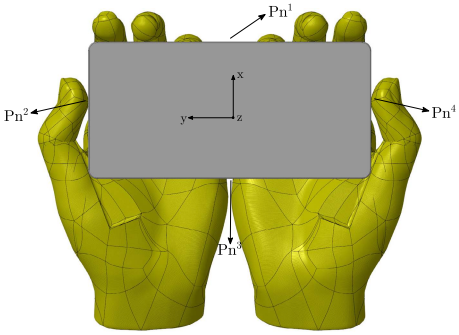

FIGURE 9. Dual hand grip model 1 - landscape mode.

video calls. This study also includes dual-hand grips, since a large number of device applications nowadays require the phone to be used in landscape mode, which, due to large form factor sizes, is usually done with both hands. Since handling of the phone is subjective to each user, countless grips could be considered. In this paper an attempt to categorize dual hand grips is made by selecting a moderate and severe grip in terms of blockage impact. Fig. 9 displays dual hand grip model 1, a pessimistic grip where the hands engulf a large area of the smartphone, which can occur when the user is streaming content. Here both Pn^2 and Pn^4 are slightly covered by the users thumbs, while Pn^1 and Pn^3 are partially blocked by the user's fingers and palms, respectively. Dual hand grip model 2 mimics a gaming stance where the user is interacting with the screen, as shown in Fig. 10. Both Pn^2 and Pn^4 are completely ensnared by the hands, while Pn^1 and Pn^3 remain uncovered. These hand grips are replicated in CST as variations of the Wide Hand Grip computer-aided-design (CAD) model defined and supplied by the Cellular Telecommunications and Internet Association (CTIA) [32] with $\varepsilon_r = 16.5$ and $\sigma = 25.8\,\mathrm{S\,m^{-1}}$, as shown in Table 3 [20].

IV. MODEL COMPARISON

This section highlights the main differences between the 3GPP and CST antenna and user blockage models. While

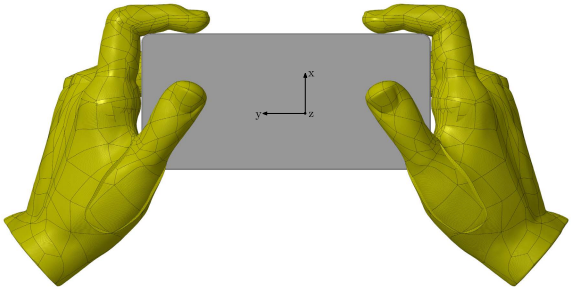

FIGURE 10. Dual hand grip model 2 - landscape mode.

Subsection IV-A compares the two model approaches on a per-antenna element basis, Subsection IV-B describes the human blockage model impact on a narrow UE beam codebook.

A. ANTENNA AND BLOCKAGE MODEL COMPARISON

The 3GPP model assumes that all antenna elements in an array share the same radiation pattern, $G_{ae}(\theta, \phi)$, described in Subsection III-A1. In reality, each antenna element's pattern depends on its placement in the form factor. Its proximity to other device components and its coupling to adjacent antennas creates a unique radiation pattern for each element, affecting the array's beam shape. This phenomenon is better captured with CST, where it is possible to extract the individual radiation patterns of each antenna in a panel array, resulting in a more realistic combined beam pattern.

However, the repercussions of such a simplification to the model become exacerbated when accounting for the user's self-blockage. In the presence of a hand grip, each antenna in each panel experiences a separate level of blockage, depending on how the hand falls onto the device. It is possible that some antenna elements in a panel are fully or partially covered by a finger while others remain undisturbed. How close together the user's fingers are, as well as their distance to the panel also impacts the performance of each element differently, potentially leading to a complete loss of the original beam shape. However, the current 3GPP model for self-blockage assumes the same blocking region for all panels, with all antennas suffering the same attenuation. Moreover, this model does not account for blockage-induced beam pattern deformation. The beams still resemble the blockage-free scenario except for a fixed attenuation area. The contrast between both models is discernible in Fig. 11, where the radiation patterns for Pn^1's antenna element 1 and antenna element 4 are considered under the portrait blockage models. While the radiation patterns of the 3GPP model are indistinguishable, there is a clear discrepancy between the antennas in the CST model. For this grip, as seen in Fig. 8, the thumb of the user rests over Pn^1. Although not visible in the illustration, antenna element 1 is the closest to the base of the thumb, being more affected than antenna element 4.

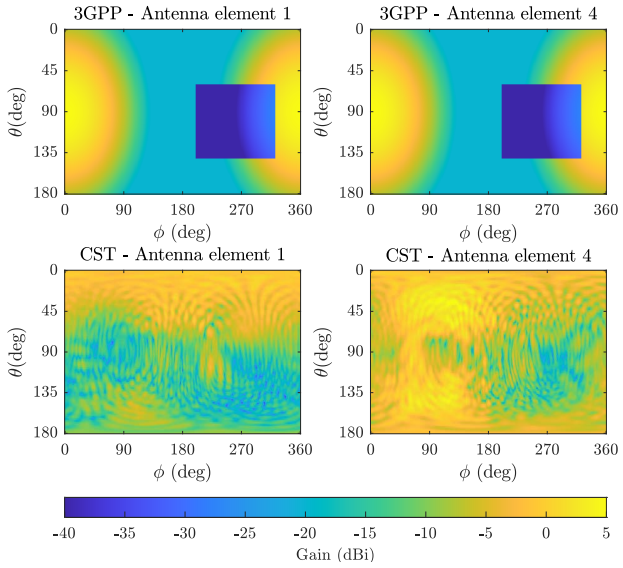

FIGURE 11. Radiation patterns of Pn^1's antenna elements 1 and 4 for portrait mode blockage - 3GPP and CST models.

Therefore, 3GPP's approach of keeping the same blockage assumption per panel could lead to misleading results. Instead, CST is closer to reality since it can use CAD models for any user body part, better characterizing the variability of a user's behavior through a wider range of blockage regions. Despite not constituting a generalized model like the ones in [19] or [20], the CST blockage model adopted in this work portrays commonly employed handset designs and user behaviors. Considering that such standardized models are yet to be proposed, these can be used as representative use-cases to complement the simpler blockage model proposed by 3GPP.

B. CODEBOOK COMPARISON

In this work, a codebook of 20 narrow UE beams is selected, with $N_{csi} = 5$ beams per panel. These narrow beams are employed during P3 to refine the UE's wide beam of the panel selected in P1. Considering now user shadowing, each blockage scenario will affect the UE's radiation behavior differently, resulting in a unique codebook shape. To evaluate blockage impact, the radiation pattern envelope of all beams is displayed as a stereographic projection in Fig. 12 for each 3GPP and CST blockage scenario. The plots are organized such that each column represents a panel, from Pn^1 through Pn^4, and each row one of the considered blockage scenarios. The first three rows represent the codebooks obtained with 3GPP's model. As a baseline, the first row depicts the free space (FS) codebook, to offer a reference of the ideal spatial coverage of the model. The following row depicts the portrait's blockage (BL) codebook followed by the landscape BL codebook in the row below. The same structure is followed for the last four rows, dedicated to the CST model. Here, the last two rows depict the two landscape BL models, models 1 and 2, detailed in Section III-B3.[2]

1) 3GPP MODEL CODEBOOK

In free space, 3GPP's codebook presents ideal and symmetrical beam shapes, with a significant gain reduction over the upper and lower bounds of elevation, as seen in the first row of Fig. 12. This model's portrait blockage, represented in the second row, covers partially Pn^1 and Pn^3 and completely blocks the highest gain region of Pn^4, leaving Pn^2 unscathed. The blockage for the device in landscape mode, illustrated in the following row, however, reaches out to all the panels, conceiling most of Pn^1 and Pn^2 and slightly blocking Pn^3 and Pn^4.

2) CST MODEL CODEBOOK

CST's free space codebook, displayed in the forth row of Fig. 12, despite employing antennas designed to resemble the 3GPP model, produces wider beams with slightly less gain, due to the power dissipating towards the edges of the metallic form factor, providing a more uniform spherical coverage. However, the proximity of the user to the mmWave antenna arrays integrated in the phone, allied with the glass acting as a wave guide and trapping some of the energy before it bounces around and escapes, can cause standing waves, making the narrow beams lose power and shape with a severity dependent on the grip conditions. Furthermore, the close contact of the panel with the device's metal structure and glass explains the ripple effects observed in the CST radiation patterns, not present in the 3GPP model. The fifth row of Fig. 12 represents the portrait mode blockage scenario from Fig 8. Since the user's thumb is pressed against Pn^1, its codebook becomes severely affected. Pn^2, on the other hand, barely registers any disturbance, being too far from the hand to produce any significant degradation. Pn^3 is also blocked to some extent but the fingers are quite spaced apart, allowing the panel to conserve part of its beam shape. While it is possible for Pn^3 to radiate almost undisturbed in the top hemisphere of elevation, this does not happen for the bottom hemisphere, where a drastic loss of power takes place in the region of the phone engulfed by the hand. Finally, in Pn^4, thanks to a small gap between the user's hand and the form factor, the main beams are able to maintain a regular shape and even experience an increase in power due to reflections coming from the user's palm. However, some attenuation is still observed in the backlobe region since, at these frequencies, the panel is unable to radiate through the hand cupping the phone. In the following row, landscape grip model 1's codebook from Fig. 9 can be found. Since both hands are cupping the phone, Pn^2 and Pn^4 patterns are mostly lost for the region above 45° of elevation. Pn^1 beams are able to keep their shape but the backlobes are attenuated due to the hand's position.

[2]While the color scale in Figure 12 has been restricted to be between −15 dB and 10 dB for clarity reasons, higher and lower gain values are obtained in some cases.

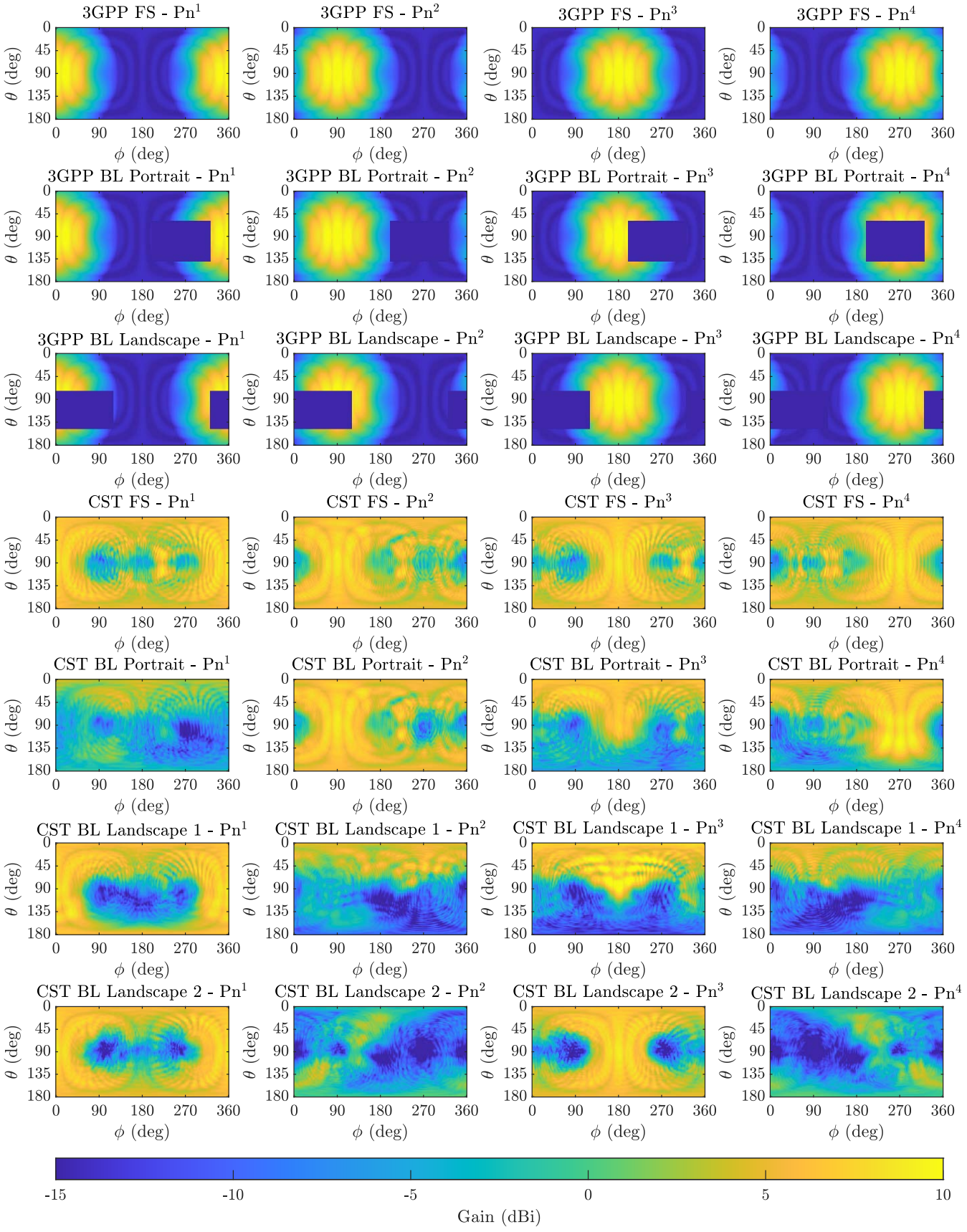

FIGURE 12. 3GPP and CST 5-beam panel codebook envelopes for free space (FS), portrait and landscape blockage (BL).

TABLE 4. Panel blockage.

Blockage scenario	Most affected panels
3GPP BL portrait	$Pn^4 > Pn^3 > Pn^1 > Pn^2$
3GPP BL landscape	$Pn^1 > Pn^2 > Pn^4 > Pn^3$
CST BL portrait	$Pn^1 > Pn^3 > Pn^4 > Pn^2$
CST BL landscape 1	Pn^2 , $Pn^4 > Pn^3 > Pn^1$
CST BL landscape 2	Pn^2 , $Pn^4 > Pn^1$, Pn^3

Pn^3 suffers a similar effect to Pn^4 in portrait mode, where most of its radiation is completely blocked by the user's palms except for the top area of elevation where some reflections are recorded. Finally, the last row displays the codebook for the landscape grip model 2 depicted in Fig. 10. The attenuation experienced in Pn^2 and Pn^4 is further aggravated, with the beam shapes almost lost in their entirety. This new grip places the user's hands near the top and bottom of the phone, freeing up Pn^1 and Pn^3 to radiate very similarly to the free space scenario. For reference in the studies that follow, Table 4 details which panels are affected by human blockage and to what extent they are blocked relative to the remaining panels in each blockage scenario.

In summary, the main contrast between the models is how user blockage is characterized:

- The 3GPP model adopts the same blockage region and attenuation values in all panels, resulting in harsher losses over a limited angular region, while the remaining angular space is unaltered when compared to free space.
- In the CST model, where each panel is affected differently by the hand positioning, the hand grip blockage manifests as a disturbance along the entire angular range but rarely displays as drastic attenuation values as its 3GPP counterpart.

V. BM PERFORMANCE EVALUATION

This section explores the impact of self-blockage in the link-level performance of BM. The key performance indicators (KPIs) used are defined in Subsection V-A. Subsection V-B and Subsection V-C showcase how RSS and beam detection accuracy are influenced by CST and 3GPP's user grip models. Finally, Subsection V-D evaluates how the channel's LOS conditions can affect blockage impact perception. Table 5 summarizes all the simulation parameters used. This study is conducted at $f_c = 28\,\text{GHz}$ with a bandwidth of $B = 104\,\text{MHz}$. Using an 8×8 UPA at the gNodeB side, BM performance is evaluated over a Urban Micro (UMi) channel model with a distance dependent LOS probability [19].

A. KPIs

To evaluate BM performance, RSS measurements are performed over the time-frequency resources reserved for data transmission. This work assumes a data resource allocation set, $\mathcal{K}_{data}$, to occupy, in the frequency domain, all the available bandwidth B, and, in the time domain, the interval

TABLE 5. Simulation parameters.

Parameter	Notation	Value
Carrier frequency	f_c	28 GHz
Carrier bandwidth	B	104 MHz
Subcarrier spacing	Δf	120 KHz
RX noise figure	NF	9 dB
Thermal noise density	N_0	$-174\,\text{dBm Hz}^{-1}$
SSB configuration		
SSBurst size	N_{ss}	12
SSBurst periodicity	T_{ss}	20 ms
SSBs for CR1	N_{ss}^{CR1}	4
SSBs for CR2	N_{ss}^{CR2}	8
CSI-RS configuration		
Resources	N_{csi}	5
Configuration row	-	1
Type	-	NZP
Resource bandwidth	-	72 PRB
density	ρ	3
Layout configuration		
Inner mobility bound	r	15 m
Outer mobility bound	R	100 m
Channel model	-	UMi LOS probability
gNodeB position	(x, y)	$(0, 0)$
gNodeB height	h_t	10 m
gNodeB array size	N_t	8×8
UE initial position	(x, y)	uniformly distributed
UE height	h_r	1.5 m
UE panels	I	4
UE panel size	N_r	1×4
UE speed	v	$3\,\text{km h}^{-1}$
UE trajectories	-	800

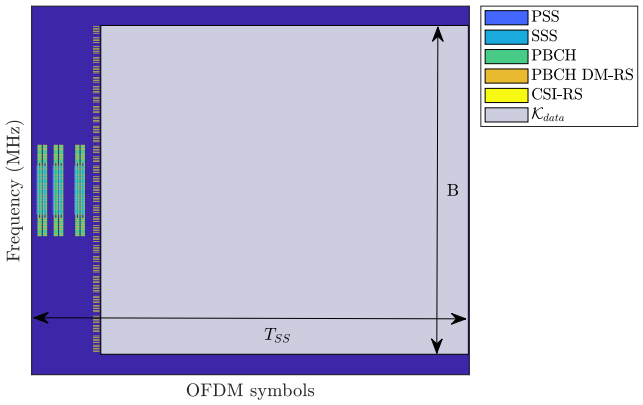

FIGURE 13. Data time-frequency allocation.

that follows the last CSI-RS transmission from P3 and the following SSBurst, as displayed in Fig. 13. The RSS over $\mathcal{K}_{data}$ for a gNodeB beam ψ_t and a UE beam ψ_r at panel i is defined as

$$R(\psi_t, i, \psi_r) = \frac{1}{|\mathcal{K}_{data}|} \sum_{k \in \mathcal{K}_{data}} |\boldsymbol{w}_{\psi_r}^H \boldsymbol{H}^i(k) \boldsymbol{f}_{\psi_t}|^2, \quad (22)$$

where $|\mathcal{K}_{data}|$ denotes the cardinality of set $\mathcal{K}_{data}$, i.e., the amount of time-frequency resources available for

data transmission. The best measurement-based beam pair is defined by the gNodeB and UE panel beam combination that offers the highest L1-RSRP levels, given by

$$R_{meas} = R(\psi_t^\star, i^\star, \psi_r^\star), \tag{23}$$

where $\psi_t^\star$, $i^\star$ and $\psi_r^\star$ are determined through the P1 and P3 procedures detailed in Subsection II-B. To evaluate beam selection accuracy, the measured RSS is compared to a genie-aided beam selection. Considering optimal beam alignment, the maximum achievable RSS over all the $N_{ss} \times I \times N_{csi}$ available beam pairs is determined by

$$R_{genie} = \max_{\psi_t, i, \psi_r} R(\psi_t, i, \psi_r). \tag{24}$$

It is considered that a beam misdetection occurs when the measurement selected gNodeB beam, UE panel or UE panel beam stray from the genie selection, based on optimal RSS results. Misdetection probability is then defined as

$$P_m = \mathbb{P}[R_{meas} < R_{genie}]. \tag{25}$$

The impact of misdetections can vary, depending on the degree of misalignment between the measured beam pair and the genie solution. An additional criterion is introduced to quantify the beam misdetection loss, given by

$$\Delta SNR = \frac{R_{genie}}{R_{meas}}. \tag{26}$$

To distinguish which misdetections risk jeopardizing communications, $P_{m_{thrdB}}$ expresses the probability that the ΔSNR incurred exceeds a threshold thr dB as

$$P_{m_{thrdB}} = \mathbb{P}[\Delta SNR_{dB} \geq thr]. \tag{27}$$

B. HAND GRIP IMPACT

It has been established in Section IV-B that a user's hand gripping can largely impact the beam shapes of a UE codebook. It remains now to be investigated to which extent this will degrade the BM performance. Considering each blockage scenario as a distinct codebook to be compared against the one originally designed for free space, Fig. 14 shows the resulting RSS obtained for each codebook after measurement-based beam alignment, under 3GPP and CST modelling assumptions. The free space scenario is characterized by two distinct curves, one for the device in portrait mode and another for the device in landscape mode, due to the different rotations introduced to the UE in each mode. To ease interpretation, Table 6 pinpoints the most significant values on the 10^{th}, 50^{th} and 90^{th} percentiles. For free space, the 3GPP and CST models produce quite similar results, which is to be expected considering these models should match. It is noticeable that the 3GPP portrait blockage curve does not stray too far from the baseline, despite being characterized by such a substantial attenuation. This can be explained by how often each UE panel is selected. Fig. 15 and Table 7 indicate, for each blockage scenario, a visual and tabular representation of the selection

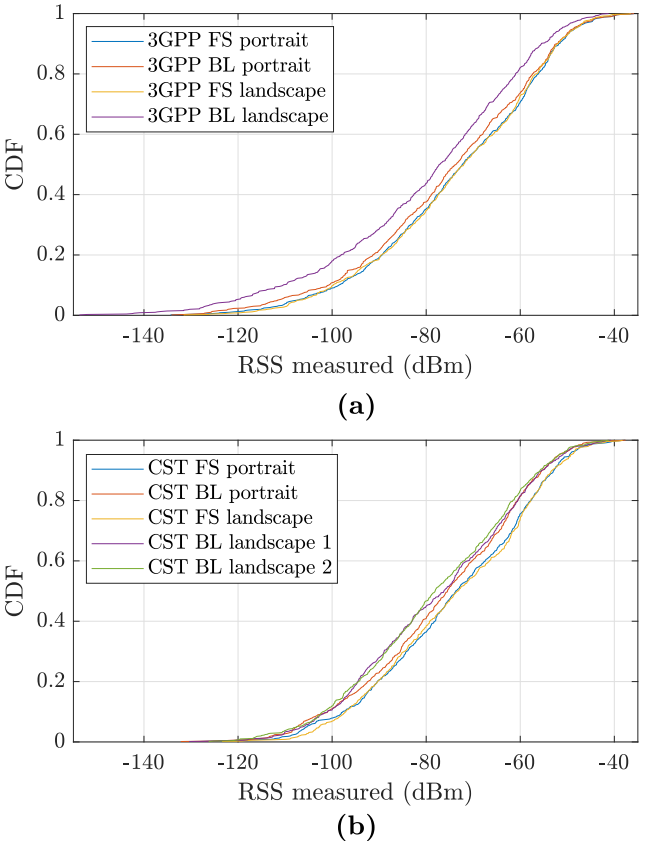

FIGURE 14. Measurement-based RSS (R_{meas}). (a) 3GPP model. (b) CST model.

TABLE 6. R_{meas} values in dBm for the 10^{th}, 50^{th} and 90^{th} percentiles.

	Percentile		
Blockage scenario	10^{th}	50^{th}	90^{th}
3GPP FS portrait	−98.6	−72.3	−51.5
3GPP BL portrait	−100.7	−73.7	−52.3
3GPP FS landscape	−99.7	−72.0	−52.0
3GPP BL landscape	−110.4	−77.2	−55.5
CST FS portrait	−97.1	−73.2	−52.9
CST BL portrait	−101	−75.5	−55.4
CST FS landscape	−97.1	−73.2	−53.2
CST BL landscape 1	−101	−76.2	−55.5
CST BL landscape 2	−102	−78.1	−55.8

percentage of each panel. An increased frequency of use for a panel is indicative of its role in achieving the best possible performance.

Results show that, for free space in portrait mode, Pn^1 and Pn^3 are selected more than 60 % of the time. Fortunately, the panel most affected by 3GPP's portrait blockage is Pn^4, which bears the lowest usage percentage in free space. Since Pn^3 is also partially blocked, its usage drops around 2 %, but is compensated by the second and third most used panels, Pn^1 and Pn^2, which justifies the small but visible performance deterioration. In landscape mode, however, the blockage impact is a lot more flagrant. The panels blocked

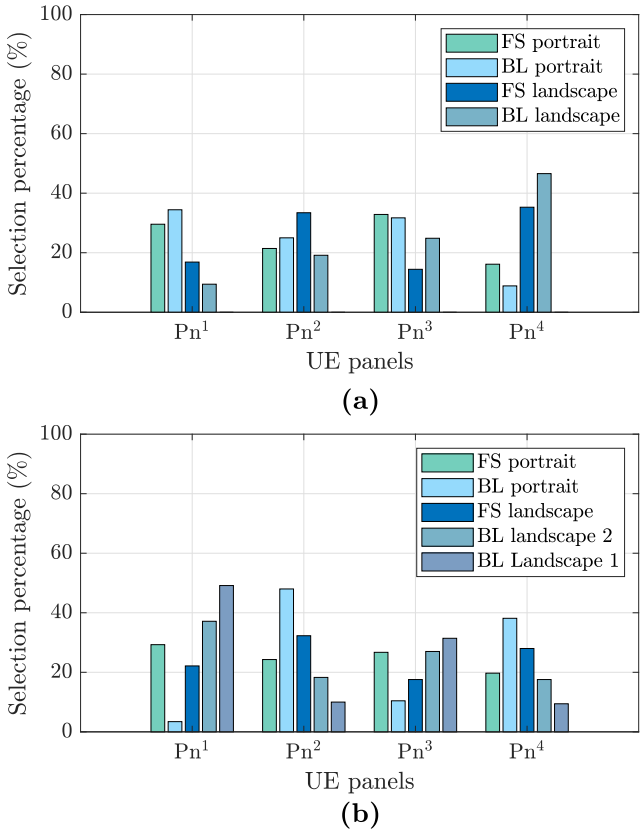

FIGURE 15. Panel selection frequency for all blockage scenarios. (a) 3GPP model. (b) CST model.

TABLE 7. Panel selection frequency for all blockage scenarios.

		Selection percentage (%)			
		Portrait		Landscape	
		FS	BL	FS	BL 1 / BL 2
Pn^1	3GPP	30.9	34.4	17.1	9.7
	CST	29.6	3.2	22	37.1 / 49.1
Pn^2	3GPP	21.1	24.7	33.1	19.3
	CST	23.5	47.1	31.9	18.3 / 10
Pn^3	3GPP	33.3	31.5	15.2	24.5
	CST	27.5	10.3	17.9	27.1 / 31.4
Pn^4	3GPP	14.7	7.5	34.7	46.3
	CST	19.5	39.5	28.3	17.6 / 9.4

more critically are Pn^1 and Pn^2, the latter being one of the most frequently employed panel in free space. As a result, the usage of these two panels is significantly reduced and substituted by an increase of activity in Pn^4, the most used panel in free space, and Pn^1, the least resorted to panel in the list, causing the performance degradation observable in Fig. 14 a).

Since CST in free space offers a more uniform coverage, the distribution of the panel selection is more balanced. Pn^1 and Pn^3 still remain as the most used panels but only by a smaller margin. Due to being largely blocked, Pn^1 is selected nearly ten times less than in the baseline. The same behavior is noticeable for Pn^3, recording a 17 % drop in its usage. The least utilized panels, Pn^2 and Pn^4 emerge as the available alternatives, which explains the deterioration of the signal. For free space landscape mode, Pn^2 and Pn^4 are chosen the most. However, for both CST landscape blockage grips, these are also the two most blocked panels, with a different level of blockage for each grip. Since the best panels are blocked, the remaining less optimal ones are selected more often instead, bringing about the observed loss in power. The performance for hand grip model 2 is even inferior to hand grip model 1 due to the extreme blockage that the gaming grip inflicts on Pn^2 and Pn^4, rendering these panels almost unusable. This reduces even further their usage percentage, resulting in higher RSS losses. It is also noteworthy that, even when largely blocked, some panels can still be selected, instead of being discarded from the candidate list, which is a common strategy adopted in prior work.

Overall, the 3GPP blockage model results in a more significant performance degradation in the worst case scenarios, represented by the lowest percentiles in Fig. 14 a). CST's model, however, leads to a more homogeneous degradation across the RSS range, as depicted in Fig. 14 b). In summary, hand grip blockage does impact negatively the performance of mmWave BM and should not be disregarded when designing such solutions for user handled devices.

While the current BM procedure appears somewhat resilient to codebook distortions introduced by blockage, it is important to note that the current implementation of this procedure is based on an exhaustive approach, where all panels and a large number of beams are measured, leaving less room for mistakes, under the limitations of our set-up. In future 5G and 6G releases, where the inevitable transition to the higher frequency spectrum will call for larger codebooks of narrower beams, such a strategy may become much less viable [2]. If more sophisticated grip-aware solutions were to be developed for BM that relied, for example, on identifying blocked panels for optimal beam selection such as [33], the variability of the user grips would make this process more prone to mistakes. Moreover, if these algorithms were to be developed under the current 3GPP blockage model assumptions, due to the lack of nuance of attenuation values and shadowing regions for different grips, it is likely that such solutions would not perform as expected in real-life scenarios. Therefore, it is necessary to consider more accurate blockage models in order to effectively counteract the impact of user influence in mmWave communications.

C. BEAM DETECTION ACCURACY

The previous results show the performance of measurement-based beam selection. This selection process, however, is always vulnerable to mistakes that can occur during the BM procedure. In this context, a misdetection can take place when either a non-ideal gNodeB beam, UE panel or UE

TABLE 8. Misdetection probability for all blockage scenarios under different loss thresholds.

Blockage scenario	$P_m(\%)$	$P_{m_{3dB}}(\%)$	$P_{m_{10dB}}(\%)$
3GPP FS portrait	74.4	37.3	16.7
3GPP BL portrait	76.1	40.6	19.9
3GPP FS landscape	72.9	36.9	17
3GPP BL landscape	77.3	44	26.6
CST FS portrait	81.1	42.7	15
CST BL portrait	84.7	48.4	17.7
CST FS landscape	80.6	42.9	14.1
CST BL landscape 1	83.9	49.3	21.3
CST BL landscape 2	81.7	48.6	21.1

panel beam are selected. It is then worth to investigate how often these misdetections occur, what is the loss incurred for such mishaps and how user blockage influences these results. Table 8 contains the P_m, $P_{m,3dB}$ and $P_{m,10dB}$ obtained for each blockage scenario. Overall, P_m results show that misdetections occur quite regularly. This is partly due to the fact that narrow beams are being considered on both the gNodeB and UE sides, making the criteria for optimal beam selection increasingly stringent. Moreover, this surprisingly large number of misdetections is also caused by the usage of a distance-dependent UMi LOS channel model. Due to users' position being uniformly distributed in the cell area, it is more likely for users to be further away from the gNodeB than closer. As users with larger distance to the gNodeB have larger probability of being in no-line-of-sight (NLOS) conditions, this is the predominant condition in the simulation, thus increasing the chances for a misdetection. However, the percentage of misdetections that actually lead to a sub-optimal link with a half-power degradation is much lower, as seen by the values registered for $P_{m_{3dB}}$. It is also noticeable that the CST model is more susceptible to misdetections than 3GPP's, which might be attributed to the nuances between their codebooks. It has been established that, due to the presence of the form factor in free space and the user's hand grip, beams become slightly warped, due to the redirection and absorption of the radiated power, creating a codebook of beams with less gain but more coverage. Therefore, since the power is better distributed over the angular space, it is more likely that there are more beams offering similar power levels, leading to misdetections. The 3GPP codebook retains its ideal shape, even when blockage is considered, only suffering a flat attenuation in a predetermined region. However, the values in $P_{m_{10dB}}$ seem to suggest a conflicting trend, where 3GPP performs worse. To explore this further, Fig. 16 represents the misdetection-induced signal-to-noise ratio (SNR) losses for each blockage scenario. Despite suffering fewer misdetections, 3GPP's SNR loss range is much larger than CST's. This is due in part to the ideal shape of 3GPP beams in free space, having no backlobes and very low power in the upper and lower bounds of elevation, as opposed to CST. This, combined with the considered blockage model, can produce large power losses when a misdetection takes place, bringing to light the

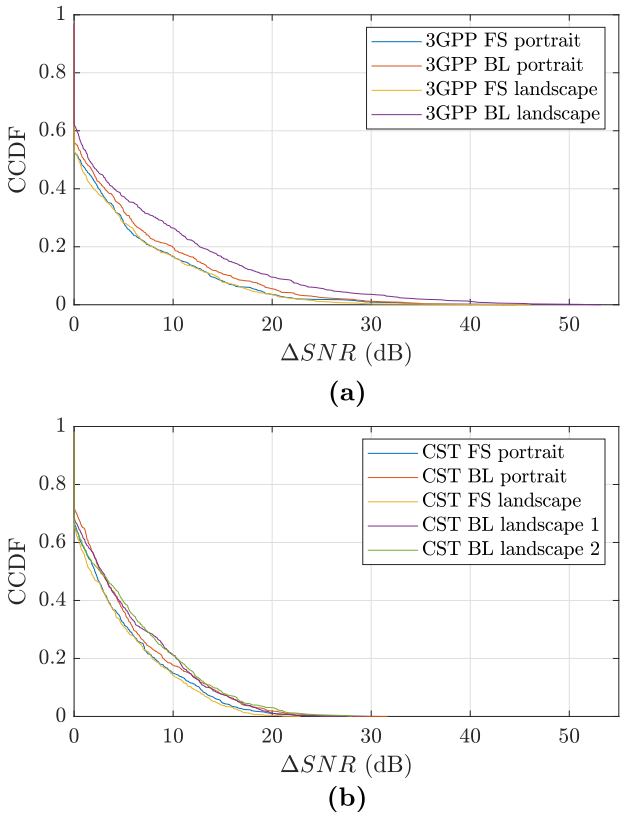

FIGURE 16. *SNR* **loss for all blockage scenarios. (a) 3GPP models. (b) CST models.**

main drawback of this model's over-pessimistic depiction of attenuation. Therefore, even though misdetections are rarer under 3GPP modelling, these become considerably more significant than in CST, potentially triggering unnecessary radio link failures. Finally, it is abundantly clear that, for both models, misdetections tend to increase with the amount of blockage incorporated, which further demonstrates how user blockage must be considered when assessing mmWave BM performance.

D. CHANNEL MODEL IMPACT

So far, results have been computed using the 3GPP-defined UMi channel model with a LOS probability dependent on the UE's distance to the gNodeB. This would resemble a more realistic urban environment where users closer to the gNodeB would be more likely to find an unobstructed link than users placed further away in the cell. However, comparing this channel model with a strict LOS or NLOS UMi channel can provide some insightful information on how blockage is perceived in different channel models. This study focuses solely on CST grips since they are deemed in this paper as the most appropriate method to gauge user blockage impact. Fig. 17 displays the measured RSS for free space, portrait blockage and landscape blockage 1 over each channel model, having NLOS described by dotted-dashed lines, LOS probability with solid lines and finally LOS with dashed lines.

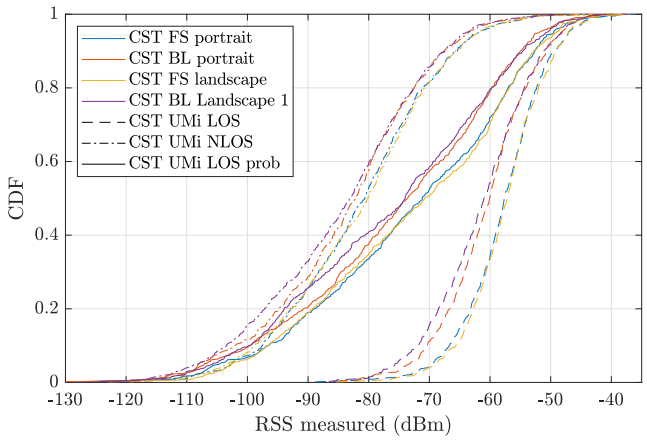

FIGURE 17. Measurement-based RSS (R_{meas}) for all UMi channel models.

TABLE 9. Misdetection probability for all UMi channel models.

	P_m(%)		
Blockage scenario	LOS	LOS prob	NLOS
CST FS portrait	67.5	80.5	90.8
CST BL portrait	73.7	84.6	90.2
CST FS landscape	68	79.5	90
CST BL landscape 1	73.2	82.8	91.6

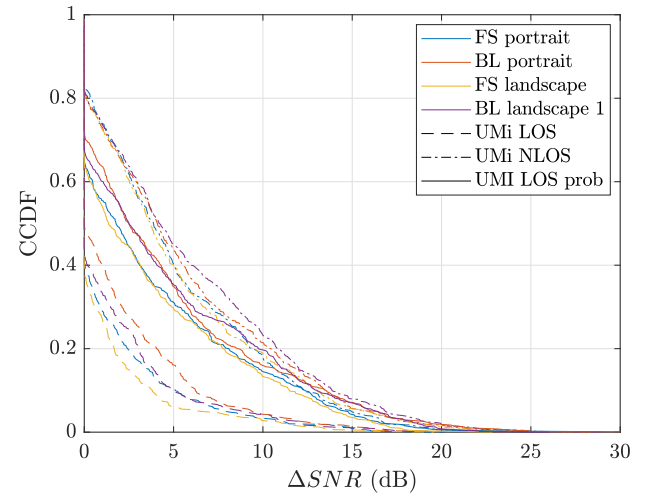

FIGURE 18. *SNR* loss for all UMi channel models.

The most striking observation lies in the fact that UMi with LOS probability curves share their lower bounds with UMi NLOS and upper bounds with UMi LOS, indicating that having a cluster rich environment negatively impacts BM performance. This is further corroborated by the P_m values in Table 9, where the misdetection probability increases significantly as the channel model transitions from a dominant LOS path channel to an obstacle rich one. This trend holds true for ΔSNR as well, as seen in Fig. 18.

Furthermore, the influence of user blockage is more visible in LOS than for the other two channel models, since in this environment there are fewer reflections to rely on once a panel is blocked. Therefore, opting for an alternative beam pair link when the optimal one is blocked results in a larger degradation than in NLOS, where a signal is already weak, even without the blockage effect.

It is important to note that, besides LOS conditions, the blockage impact assessment results are also dependent on factors such as gNodeB height and device rotation in the 3D space, since these would also alter the angles of arrival of the signal. Another factor that was not explored in this work but could also be important to consider in future studies, depending on the user's body orientation relative to the gNodeB, would be the blockage from the user's torso.

VI. CONCLUSION

This work has presented a link-level analysis of the impact of high-detail hand grip blockage in mmWave BM performance of handheld devices. Results showed that hand grip type, UE orientation, panel distribution in the form factor, channel conditions and network layout are all determining factors to gauge the severity of a user's blockage effect and must be carefully modeled when designing solutions to counteract hand blockage and assessing the viability of mmWave communications. While it has been shown that hand blockage noticeably degrades the BM procedure, the current 5G system signaling mechanisms are robust enough to provide sub optimal, yet acceptable, link level performance, even without any proactive measures to mitigate it. However, in future 5G and 6G releases, larger codebooks with narrower beams will likely be employed to handle the transition to higher frequencies, making sweeping-based beam selection implementations impractical. Smarter hand grip and terminal housing-aware mechanisms, such as those in [33], [34], and [35], should be adopted to create robust solutions to realistic mmWave propagation challenges. In order to enable such approaches, adequate blockage models must be agreed upon to capture the signal's absorption, reflection and diffraction effects.

A. OUTLOOK

This study's results further suggest that the current stochastic 3GPP self-blockage model [19], perhaps sufficient for system-level evaluations, lacks detail to properly portray user hand grip effects on a link-level basis, leading to an overly pessimist performance degradation. While beyond the intended scope of this work, the task of proposing a simple yet realistic hand-grip induced blockage model would be the next logical step for future work. The CST model employed in this work is quite useful to numerically assess specific UE designs and hand grip modes but lacks the generality to become a viable model for algorithm design. A CST-based approach could still be used to create a more realistic blockage model than 3GPP's, since it is able to simulate the human body and its behavior with a remarkable level of detail. However, it would require countless computationally heavy simulations to recreate different body blockage scenarios and capture the

nuances of the user's behavior in the antenna performance, which can be deemed as an impractical method. Alternatively, an improvement to the current flat 30 dB attenuation model could be envisioned to establish a standard form factor design and panel placement, as the one considered in this paper, but with a statistical attenuation model instead, as introduced in [20] or [21], on a per panel-basis.

REFERENCES

[1] Y.-N.-R. Li, B. Gao, X. Zhang, and K. Huang, "Beam management in millimeter-wave communications for 5G and beyond," *IEEE Access*, vol. 8, pp. 13282–13293, 2020.

[2] Y. Heng, J. G. Andrews, J. Mo, V. Va, A. Ali, B. L. Ng, and J. C. Zhang, "Six key challenges for beam management in 5.5G and 6G systems," *IEEE Commun. Mag.*, vol. 59, no. 7, pp. 74–79, Jul. 2021.

[3] Y. Huang, Y. Li, H. Ren, J. Lu, and W. Zhang, "Multi-panel MIMO in 5G," *IEEE Commun. Mag.*, vol. 56, no. 3, pp. 56–61, Mar. 2018.

[4] *CST Microwave Studio*. Accessed: Jun. 2022. [Online]. Available: https://www.cst.com/products/cstmws

[5] Y. Li, J. G. Andrews, F. Baccelli, T. D. Novlan, and J. C. Zhang, "Design and analysis of initial access in millimeter wave cellular networks," *IEEE Trans. Wireless Commun.*, vol. 16, no. 10, pp. 6409–6425, Oct. 2017.

[6] M. Rebato, J. Park, P. Popovski, E. D. Carvalho, and M. Zorzi, "Stochastic geometric coverage analysis in mmWave cellular networks with realistic channel and antenna radiation models," *IEEE Trans. Commun.*, vol. 67, no. 5, pp. 3736–3752, May 2019.

[7] A. Karimi and K. I. Pedersen, "5G system-level performance analysis of uplink multi-panel transmission in mm-wave frequencies," in *Proc. IEEE 94th Veh. Technol. Conf. (VTC-Fall)*, Sep. 2021, pp. 1–6.

[8] F. Abinader, C. Rom, K. Pedersen, S. Hailu, and N. Kolehmainen, "System-level analysis of mmWave 5G systems with different multi-panel antenna device models," in *Proc. IEEE 93rd Veh. Technol. Conf. (VTC-Spring)*, Apr. 2021, pp. 1–6.

[9] S. B. Iqbal, A. Awada, U. Karabulut, I. Viering, P. Schulz, and G. P. Fettweis, "Analysis and performance evaluation of mobility for multi-panel user equipment in 5G networks," in *Proc. IEEE 95th Veh. Technol. Conf. (VTC-Spring)*, Jun. 2022, pp. 1–7.

[10] A. Ali, J. Mo, B. L. Ng, V. Va, and J. C. Zhang, "Orientation-assisted beam management for beyond 5G systems," *IEEE Access*, vol. 9, pp. 51832–51846, 2021.

[11] K. N. Nguyen, A. Ali, J. Mo, B. L. Ng, V. Va, and J. C. Zhang, "Beam management with orientation and RSRP using deep learning for beyond 5G systems," 2022, *arXiv:2202.02247*.

[12] M. Peter, M. Wisotzki, M. Raceala-Motoc, W. Keusgen, R. Felbecker, M. Jacob, S. Priebe, and T. Kurner, "Analyzing human body shadowing at 60 GHz: Systematic wideband MIMO measurements and modeling approaches," in *Proc. 6th Eur. Conf. Antennas Propag. (EUCAP)*, Mar. 2012, pp. 468–472.

[13] U. T. Virk and K. Haneda, "Modeling human blockage at 5G millimeter-wave frequencies," *IEEE Trans. Antennas Propag.*, vol. 68, no. 3, pp. 2256–2266, Mar. 2020.

[14] K. Zhao, J. Helander, D. Sjöberg, S. He, T. Bolin, and Z. Ying, "User body effect on phased array in user equipment for the 5G mmWave communication system," *IEEE Antennas Wireless Propag. Lett.*, vol. 16, pp. 864–867, 2016.

[15] K. Zhao, C. Gustafson, Q. Liao, S. Zhang, T. Bolin, Z. Ying, and S. He, "Channel characteristics and user body effects in an outdoor urban scenario at 15 and 28 GHz," *IEEE Trans. Antennas Propag.*, vol. 65, no. 12, pp. 6534–6548, Dec. 2017.

[16] K. Zhao, S. Zhang, Z. Ho, O. Zander, T. Bolin, Z. Ying, and G. F. Pedersen, "Spherical coverage characterization of 5G millimeter wave user equipment with 3GPP specifications," *IEEE Access*, vol. 7, pp. 4442–4452, 2019.

[17] C. Ballesteros, L. Vaha-Savo, K. Haneda, C. Icheln, J. Romeu, and L. Jofre, "Assessment of mmWave handset arrays in the presence of the user body," *IEEE Antennas Wireless Propag. Lett.*, vol. 20, no. 9, pp. 1736–1740, Sep. 2021.

[18] L. Vaha-Savo, C. Cziezerski, M. Heino, K. Haneda, C. Icheln, A. Hazmi, and R. Tian, "Empirical evaluation of a 28 GHz antenna array on a 5G mobile phone using a body phantom," *IEEE Trans. Antennas Propag.*, vol. 69, no. 11, pp. 7476–7485, Nov. 2021.

[19] *Study on Channel Model for Frequencies From 0.5 to 100 GHz (Release 17)*, Standard 3GPP, TR 38.901 V17.0.0, 2022.

[20] V. Raghavan, L. Akhoondzadeh-Asl, V. Podshivalov, J. Hulten, M. A. Tassoudji, O. H. Koymen, A. Sampath, and J. Li, "Statistical blockage modeling and robustness of beamforming in millimeter-wave systems," *IEEE Trans. Microw. Theory Techn.*, vol. 67, no. 7, pp. 3010–3024, Jul. 2019.

[21] V. Raghavan, S. Noimanivone, S. K. Rho, B. Farin, P. Connor, R. A. Motos, Y. C. Ou, K. Ravid, M. A. Tassoudji, O. H. Koymen, and J. Li, "Hand and body blockage measurements with form-factor user equipment at 28 GHz," *IEEE Trans. Antennas Propag.*, vol. 70, no. 1, pp. 607–620, Jan. 2022.

[22] V. Raghavan, M.-L. C. Chi, M. A. Tassoudji, O. H. Koymen, and J. Li, "Antenna placement and performance tradeoffs with hand blockage in millimeter wave systems," *IEEE Trans. Commun.*, vol. 67, no. 4, pp. 3082–3096, Apr. 2019.

[23] S. Jaeckel, L. Raschkowski, K. Borner, and L. Thiele, "QuaDRiGa: A 3-D multi-cell channel model with time evolution for enabling virtual field trials," *IEEE Trans. Antennas Propag.*, vol. 62, no. 6, pp. 3242–3256, Jun. 2014.

[24] *Study on New Radio Access Technology Physical Layer Aspects (Release 14)*, Standard 3GPP, TR 38.802 V14.2.0, 2017.

[25] M. Enescu, *5G New Radio: A Beam-based Air Interface*. Hoboken, NJ, USA: Wiley 2020.

[26] *NR; Physical Channels and Modulation (Release 17)*, Standard 3GPP, TS 38.211 V17.3.0, 2022.

[27] *NR; Physical Layer Procedures for Control (Release 15)*, Standard 3GPP, TS 38.213 V17.3.0, 2022.

[28] *5G Toolbox*, MathWorks, Natick, MA, USA, 2019.

[29] *Feature Lead Summary #3 of Enhancements on Multi-Beam Operations*, document R1-1907860, 3GPP TSG RAN WG1 Meeting #97, LG Electronics, Reno, NV, USA, May 2019.

[30] *NR; Physical Layer Measurements (Release 17)*, Standard 3GPP, TS 38.215 V17.2.0, 2022.

[31] *Study on New Radio Access Technology: Radio Frequency (RF) and Co-Existence Aspects (Release 14)*, Standard 3GPP, TR 38.803 V14.3.0, 2022.

[32] *Test Plan for Wireless Device Over-the-Air Performance v3.8.2*, CTIA, Washington, DC, USA, Apr. 2019.

[33] A. Alammouri, J. Mo, B. L. Ng, J. C. Zhang, and J. G. Andrews, "Hand grip impact on 5G mmWave mobile devices," *IEEE Access*, vol. 7, pp. 60532–60544, 2019.

[34] J. Mo, B. L. Ng, S. Chang, P. Huang, M. N. Kulkarni, A. Alammouri, J. C. Zhang, J. Lee, and W.-J. Choi, "Beam codebook design for 5G mmWave terminals," *IEEE Access*, vol. 7, pp. 98387–98404, 2019.

[35] V. Raghavan, R. A. Motos, M. A. Tassoudji, Y.-C. Ou, O. H. Koymen, and J. Li, "Mitigating hand blockage with non-directional beamforming codebooks," 2021, *arXiv:2104.06472*.

FILIPA FERNANDES (Member, IEEE) received the B.Sc. and M.Sc. degrees in electrical and computer engineering from the Instituto Superior Técnico (IST), University of Lisbon, Lisbon, Portugal, in 2016 and 2019, respectively. She is currently pursuing the Ph.D. degree in wireless communication networks section with Aalborg University in collaboration with Nokia Standardizations, Aalborg, Denmark. Her research interests include beamforming solutions for FR2 beam management and user blockage modeling in handheld devices at mmWave frequencies.

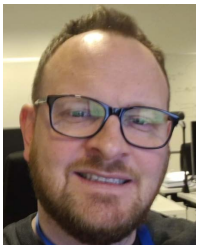

CHRISTIAN ROM received the M.Sc. degree in electrical and electronic engineering with a specialization in digital communications from Aalborg University, in 2003, and the Ph.D. degree in wireless communications. He joined Nokia-Bell Laboratories Aalborg, Denmark, in January 2019. His Ph.D. research focused on physical layer parameter and algorithm study in a downlink OFDM-LTE context. In 2022, he was awarded with the Outstanding Inventor in SIP cellular standards at Nokia. Before joining Bell Laboratories, Christian worked as the RF Innovation Manager at Intel Denmark with focus on mmWave beamforming in smartphones and production. He has 15 years' experience in the wireless industry (Intel/Infineon). During his career, he lead projects in areas such as real world modeling and virtualization from propagation, ray-tracing to comparison of the models results with on-device measurements in the field, then linking these to link level tool development, PHY receiver algorithms, and performance benchmarking and differentiation all the way to final mass scale product ramp up.

JOHANNES HARREBEK was born in 1971. He received the M.Sc. degree in electrical engineering from Aalborg University, Aalborg, Denmark, in 1995. He is currently heading the Nokia Device Standardization Research Team, Aalborg. He has 27 years of product and advanced technology development experience in the field of telecommunication and wireless systems with focus on mobile device modem RF technology analysis, optimization, simulation, design, and calibration. He has been involved in numerous cellular device development projects from 2G to 5G ranging from full end-user products over RF transceiver and modem solutions to specific RF technology offerings and also working for several well-known companies in the industry including Bosch Telecom, Siemens Mobile Phones, Analog Devices, Mediatek, and Intel Mobile Communications.

SIMON SVENDSEN received the degree from Aalborg University, in 1995, and the M.Sc.E.E. degree. He has been working in the mobile industry since then. His career started at Bang & Olufsen, where his first task was to design antennas for DECT phones and verify the RF performance of the Front End. He has since worked for Maxon, Siemens, Motorola, and Molex doing mostly cellular antenna design for mobile phones including MCAD design, EM simulations, rapid prototyping and measurement. He joined Intel, in January 2013, and has been working primarily with cellular antenna designs for internal reference platform and for customers. However, his focus in the last years at Intel, shifted towards mmWave antenna design, and the RF FE architecture. He has been employed at Nokia Bell Laboratories, since November 2018, and also working with device standardization research for 3GPP 5G NR. He has more than 50 patents within the scope of antenna designs.

CARLES NAVARRO MANCHÓN received the degree in telecommunication engineering from the Miguel Hernández University of Elche, Spain, in 2006, and the Ph.D. degree in wireless communications from Aalborg University, Denmark, in 2011. Since 2006, he has been with Aalborg University, where he is currently an Associate Professor with the Department of Electronic Systems, Wireless Communication Networks Section. His research interests lie in the area of statistical signal processing for wireless communications, including joint channel estimation and decoding algorithms, estimation and reconstruction of sparse signals, signal processing for multiple antenna systems, and machine learning methods for wireless networks.